NUMERICAL ANALYSIS OF A SHAPED RAIL PAD UNDER SELECTED STATIC LOAD

Piotr Szurgott, Paweł Gotowicki, Tadeusz Niezgoda

Military University of Technology
Department of Mechanics and Applied Computer Science
Gen. Sylwestra Kaliskiego Street 2, 00-908 Warsaw, Poland
tel.: +48 22 6839941, +48 22 6839461, fax: +48 22 6839355
e-mail: pszurgott@wat.edu.pl, pgotowicki@wat.edu.pl, tniezgoda@wat.edu.pl

Abstract

Numerical analysis of selected type of the polyurethane rail pad is presented in the paper. A shaped pad with cylindrical-shaped elements in its working section was selected as a representative for the computational simulation. Analysis reflected the experimental test according to the valid standard. The test included loading of the vertical force perpendicular to the foot of the rail. Such test allows determining the static stiffness of the pad. The Mooney – Rivlin material model was selected in the current study. Necessary experimental tests including a uniaxial compression and tension were conducted to provide material constants for the hyperelastic material model applied for the FE model. Simplified FE models of the considered rail pad and the rail were developed. Rounded corners and edges of the cylindrical-shaped elements were omitted, since their modelling required a significant density of the FE mesh. Vertical force perpendicular to the foot of the rail was declared as nodal force distributed evenly along the edges of the selected finite element models Non-linear static analysis was performed using MSC.Marc software with large displacements and deformations taken into consideration. The obtained results allowed estimating deformations and the state of stress in a highly deformed rail pad. The static stiffness of the pad was defined as secant stiffness based on the vertical force – deflection curve.

Keywords: numerical analysis, FEM, rail pad, hyperelastic material, fastening

1. Introduction

Rail fastenings including the elastic rail pads are one of the main elements of the top structure of the track. Traffic safety of the trains depends on their reliable work [1]. The main role of the elastic rail pads applied in fastening systems is to reduce the dynamic effect of the rolling railway vehicle on the concrete sleeper. They also provide an electrical insulation between the rail foot and the sleeper as well. The stiffness of a rail pad depends on the track class and the maximum track capacity. Flexible pads are applied for top class high-speed railways whereas the more stiff ones are used in second-rate tracks. Very often, the universal pads – with appropriate characteristics for every type of track – are needed to be used. Recently, more and more often classic uniform and flat pads are replaced by shaped ones with different types of the cross-section. Various types of shaped elements allow obtaining different stiffness of the pad depending on the actual rail load. Therefore, the static stiffness of the pad – which can be constant – is determined in a strictly defined range of load. Hence, a load – displacement characteristics of selected shaped pads are piecewise linear instead of linear relation for the flat ones.

A shaped pad with cylindrical-shaped elements in its working section was selected as a representative for the study described in the paper. It was made of polyurethane without any specified material parameters. Therefore, experimental including a uniaxial compression and tension had to be conducted. It was decided to choose a hyperelastic material model available in applied FEA software. Large displacements and deformations were taken into consideration since the deflection of the fully deformed pad was equal to about 15% of the pad thickness. Non-linear static analysis was performed using MSC.Marc software. The main goal of the study was to

determine deformations of the highly deformed rail pad. Moreover, numerical simulations allowed estimating the state of stress in the rail pad depending on its actual load. The results obtained for both selected pads were compared and the influence of the pad shape on its state of deformation was investigated.

FE analysis included loading of the vertical force perpendicular to the foot of the rail. Such a test allows determining the static stiffness of the pad.

2. Description of the actual pad

The elastic rail pad selected for the study is depicted in Fig. 1. Its working area includes cylindrical-shaped elements in different size and dimensions, as presented in the figure. The area is surrounded by a solid uniform "frame". The selected pad is a one-side pad and it can be used shaped-side up only.



Fig. 1. A considered pad with cylindrical-shaped elements in its working area [2]

3. Material research

As mentioned before, a selected pad was made of polyurethane. Since the material properties and its chemical constitution were not available, some experimental tests had to be conducted to obtain necessary data. Two tests – uniaxial tension and compression – were carried out using a universal strength machine INSTRON 8802.

The uniaxial tension test was carried out for 5 samples. Velocity of the machine traverse was declared according to the ASTM D412 – 98a Standard [3], and it was equal to 500 mm/min. Tension force and vertical displacement of the traverse were registered during the test. Moreover, a longitudinal strain was measured using an extensometer. Every 5 tests were conducted once the longitudinal strain reach value equalled to 200%. The results of the tension test in the form of engineering stress – engineering strain curves are presented in Fig. 2.

The uniaxial compression test was carried out for 10 cylindrical shaped samples. Diameter-to-height ratio corresponded to values recommended in the ASTM D 575 – 91 Standard [4]. Samples were compressed at the constant velocity of 50 mm/min, which was declared according to the PN-C-04253:1954 Standard [5]. The results of the compression test in the form of engineering stress – engineering strain curves are presented in Fig. 3.

The results obtained from both – tension and compression – tests were averaged and combined into one final curve depicted in Fig. 4, which was used for determination of the material constants in the hyperelastic material model.

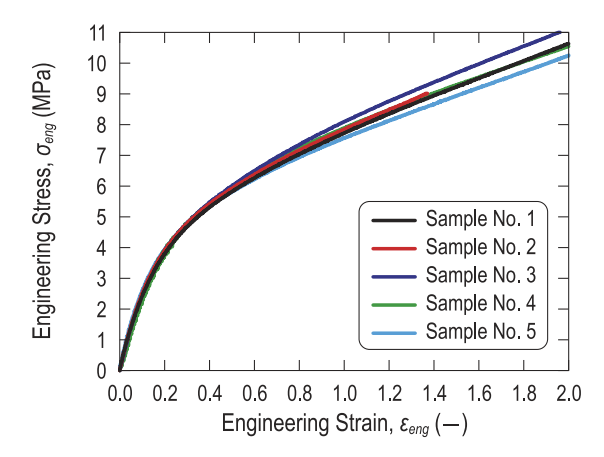


Fig. 2. Engineering stress – engineering strain curves obtained from the tension test

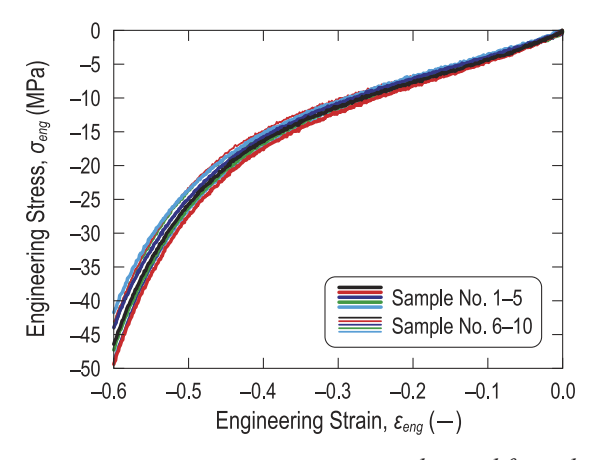


Fig. 3. Engineering stress – engineering strain curves obtained from the compression test

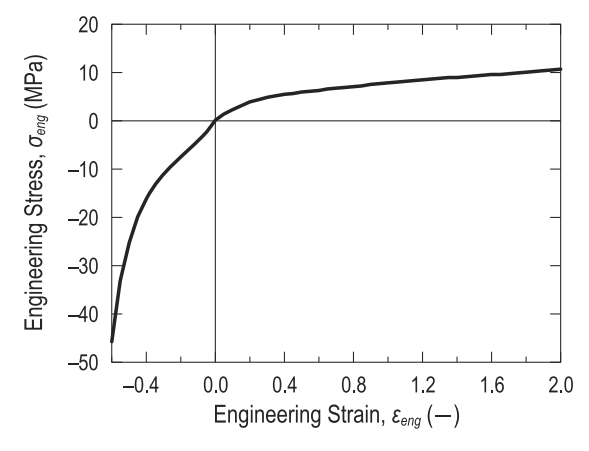


Fig. 4. The averaged engineering stress – engineering strain curve for the considered polyurethane material

4. Material model

Numerical analysis was carried out using the MSC.Marc software, which includes a module for modelling highly elastic materials, such as rubber, elastomers and others. The Mooney – Rivlin group of material models were selected in the current study. They were based on the deformation energy function W. If the term taking into account the temperature influence is omitted, the function for an uncompressible material can be written in the following polynomial form [6]:

$$W = \sum_{i+j=1}^{n} C_{ij} (I_1 - 3)^i (I_2 - 3)^j,$$
(1)

where I_1 and I_2 are deformation invariants and C_{ij} are constants defined for a particular material. The deformation invariants are given as follows:

$$I_1 = \lambda_1^2 + \lambda_2^2 + \lambda_3^2 \,, \tag{2}$$

$$I_2 = \lambda_1^2 \lambda_2^2 + \lambda_2^2 \lambda_3^2 + \lambda_3^2 \lambda_1^2 \,, \tag{3}$$

where λ_1 , λ_2 , λ_3 are elongations of the element under consideration along particular directions, as depicted in Fig. 5.

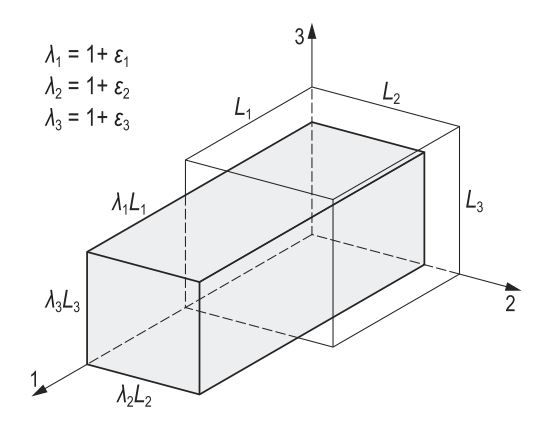


Fig. 5. Elongations λ_1 , λ_2 , λ_3 of the element under consideration in the case of uniaxial tension [7]

Constants C_{ij} expressed in Eqn. (1) were determined on the basis of the averaged engineering stress – engineering strain curve (Fig. 4). In the considered group of material models, the degree of their complexity depends on the number of constants C_{ij} . Determination of the C_{ij} constants was performed using Experimental Data Fitting algorithm included in MSC.Mentant pre-processor. It was based on the method of least squares [6]. Since the uniaxial tension/compression test results were available, it was necessary to check the model behaviour in other states, e.g. biaxial, planar shear etc. The MSC.Mentat preprocessor allows observing how the model behaves in different loading states. In order to obtain stability of the model it was necessary that C_{ij} have positive values [8].

The 2-parametr Mooney – Rivlin model with C_{10} and C_{01} constants was assumed for further analyzes. In the current study, imposing a condition of positive constants C_{ij} practically reduces all higher order material models to the model with two constants. The deformation energy function W for a selected material model is given as follows:

$$W = C_{10}(I_1 - 3) + C_{01}(I_2 - 3). (4)$$

Assuming an incompressibility of the material:

$$\lambda_1^2 \,\lambda_2^2 \,\lambda_3^2 = 1,\tag{5}$$

$$\lambda_2 = \lambda_3 = \left(\lambda_1\right)^{-1/2},\tag{6}$$

the deformation invariants can be expressed as follows:

$$I_1 = \lambda_1^2 + 2(\lambda_1)^{-1},\tag{7}$$

$$I_2 = 2\lambda_1 + (\lambda_1)^{-2}. (8)$$

Taking into consideration Eqns. (4), (7) and (8), the deformation energy W can be written in the following form:

$$W = C_{10} \left(\lambda_1^2 + \frac{2}{\lambda_1} - 3 \right) + C_{01} \left(2\lambda_1 + \frac{1}{\lambda_1^2} - 3 \right), \tag{9}$$

or

$$W = C_{10} \left((1 + \varepsilon_1)^2 + \frac{2}{1 + \varepsilon_1} - 3 \right) + C_{01} \left(2(1 + \varepsilon_1) + \frac{1}{(1 + \varepsilon_1)^2} - 3 \right). \tag{10}$$

Having defined the deformation energy W, one can determine the stress components along the directions of interest as partial derivatives:

$$\sigma_{1}(\varepsilon_{1}) = \frac{\partial W}{\partial \varepsilon_{1}} = 2 \left[C_{10} \left((1 + \varepsilon_{1}) - \frac{1}{(1 + \varepsilon_{1})^{2}} \right) + C_{01} \left(1 - \frac{1}{(1 + \varepsilon_{1})^{3}} \right) \right]. \tag{11}$$

The relation (11) is the stress – strain characteristic of the polyurethane under consideration. The results of the experimental test were approximated by the stress – strain curve for the constant value $C_{10} = 1.5218$ MPa and $C_{01} = 1.5139$ MPa (Fig. 6).

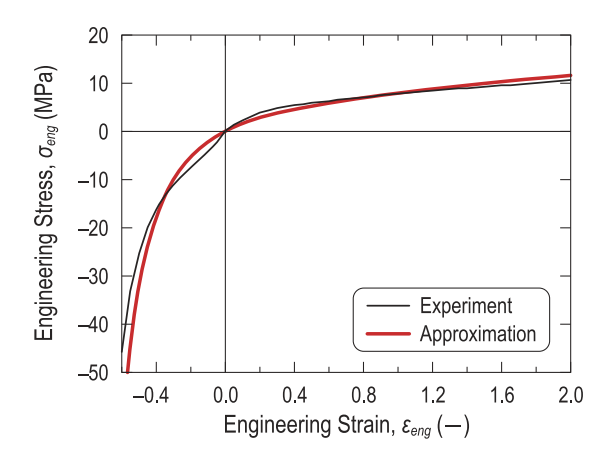


Fig. 6. Approximation of the experimental test results by 2-parameter Mooney – Rivlin material model

6. FE models

A finite element model of the quarter part of the actual system was developed (Fig. 7). Such approach was assumed, since analysis included loading of the vertical force perpendicular to the foot of the rail. Therefore, the pad was compressed and any horizontal movement or rotations of the rail were not possible. Appropriate boundary conditions resulting from the assumed symmetry were declared.

FE model of the pad did not include side protrusions providing its appropriate position between anchors of the fastening system. Rounded corners and edges of the cylindrical-shaped elements were omitted, since their modelling required a significant density of the FE mesh.

Two types of 3-D solid 8-node elements were used for modelling. A standard full integration element type 7 was applied in the rail FE model, whereas the full and Hermann formulation type 84 elements with additional ninth node were used in the pad FE model [10]. FE model of the quarter of the rail and the pad consisted of 864 and 21,354 elements, respectively. The rail and the pad components were considered as deformable bodies, whereas the sleeper was simulated as a flat rigid surface due to higher stiffness of the sleeper in comparison with the pad. The bilinear Coulomb type of friction was used in the current analysis. The friction coefficient between the sleeper and the pad was equal to 0.8, whereas between the pad and the rail foot -0.6.

Load caused by the fastening clamp was evenly distributed on the area with dimensions close to the contact zone between the rail foot and the transverse insulating rail spacer. A face load

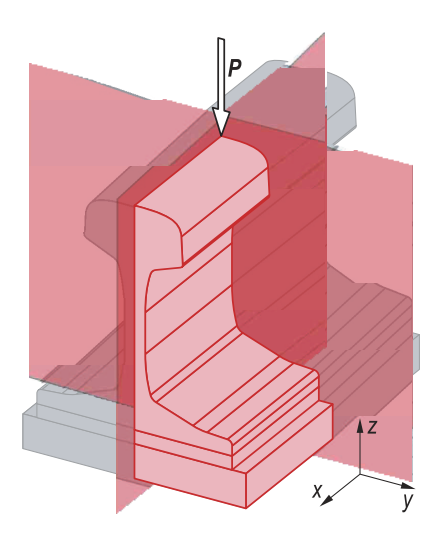


Fig. 7. Fragmentation of the actual system resulting from the assumed symmetry

option was applied in the FE model for the faces of selected elements. The maximum load corresponded to the pressure of one fastening clamp was assumed as 8 kN.

Vertical force perpendicular to the foot of the rail was declared as nodal force distributed evenly along the edges of the selected finite element models. Its value increased from 0 to the maximum declared value.

FE model of the rail – pad – sleeper system is presented in Fig. 8.

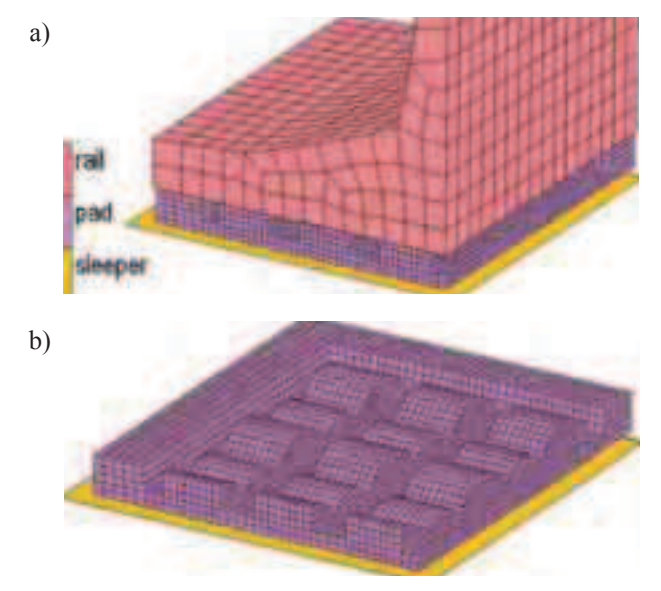


Fig. 8. FE model of the rail – pad – sleeper system (a) and FE model of the rail pad (b)

7. Results of the FE analysis

The results of numerical analysis are presented in the form of a contour band for stresses and displacements, and vertical force – deflection curve as well. The static stiffness k_{stat} of the considered pad – for the range of 16–88 kN – was defined as secant stiffness and it was determined according to the following relation:

$$k_{stat} = \frac{P_2 - P_1}{u_{P2} - u_{P1}},\tag{12}$$

where P_1 is a pressure of the fastening clamps (equal to 16 kN), P_2 is 80% of the maximum wheel load (equal to 88 kN), u_{P1} and u_{P2} are deflections of the pad under force P_1 and P_2 , respectively.

The vertical force – deflection curve is shown in Fig. 9. The secant stiffness for considered rail pad determined according to the curve depicted in Fig. 9 is equal to 70.7 kN/mm.

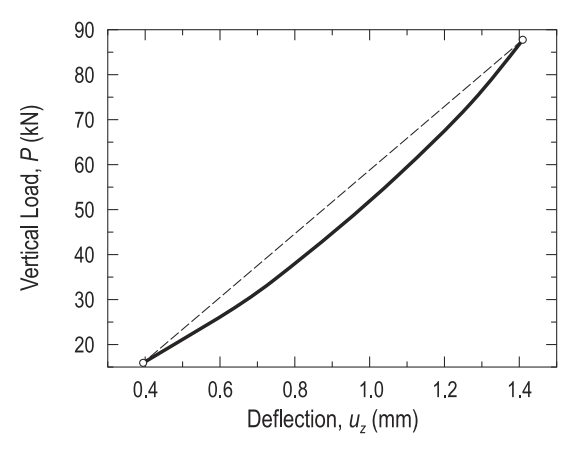


Fig. 9. The load – deflection curve obtained from the FE analysis

The contour bands of the equivalent stress and displacements for the pad under force P_1 and P_2 are presented in Fig. 10 and Fig. 11, respectively.

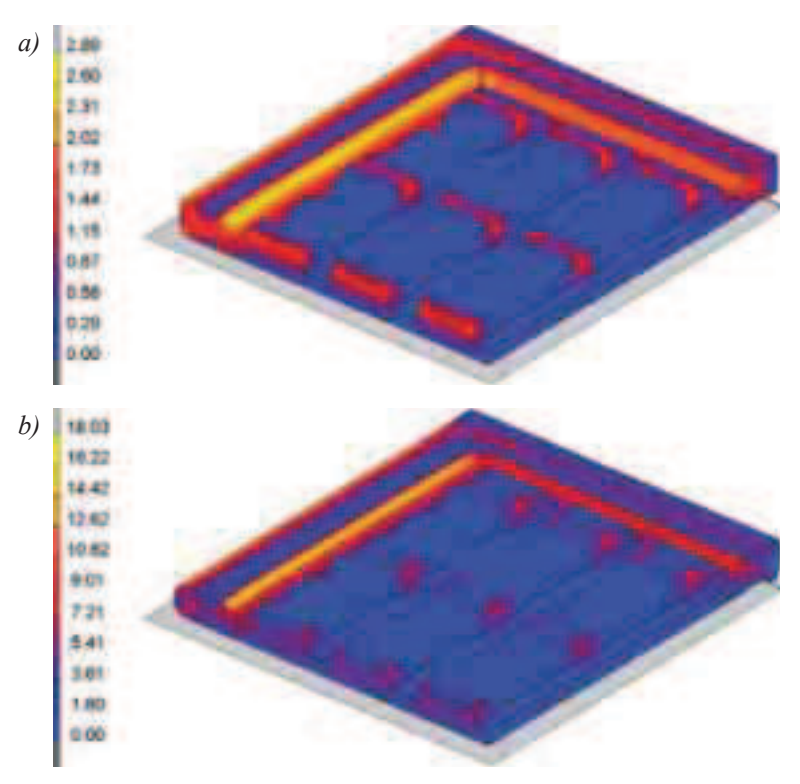


Fig. 10. Contour bands of equivalent stress (MPa) for the pad under force P_1 (a) and P_2 (b)

8. Conclusions

On the basis of the obtained results the following major conclusions may be drawn. The surrounding frame and larger cylindrical-shaped elements were only working during the compression of the rail pad. Smaller cylindrical elements were not in contact with the bottom surface of the rail foot even for the maximum load from the selected range. Therefore, the role of the universal pad was not met. The surrounding frame was responsible for the total stiffness of the pad since it took over the significant of the vertical load. It is highly probable that the influence of the cylindrical-shaped elements on the stiffness is slight. The highest stress concentrations occur at the edges of the surrounding frame.

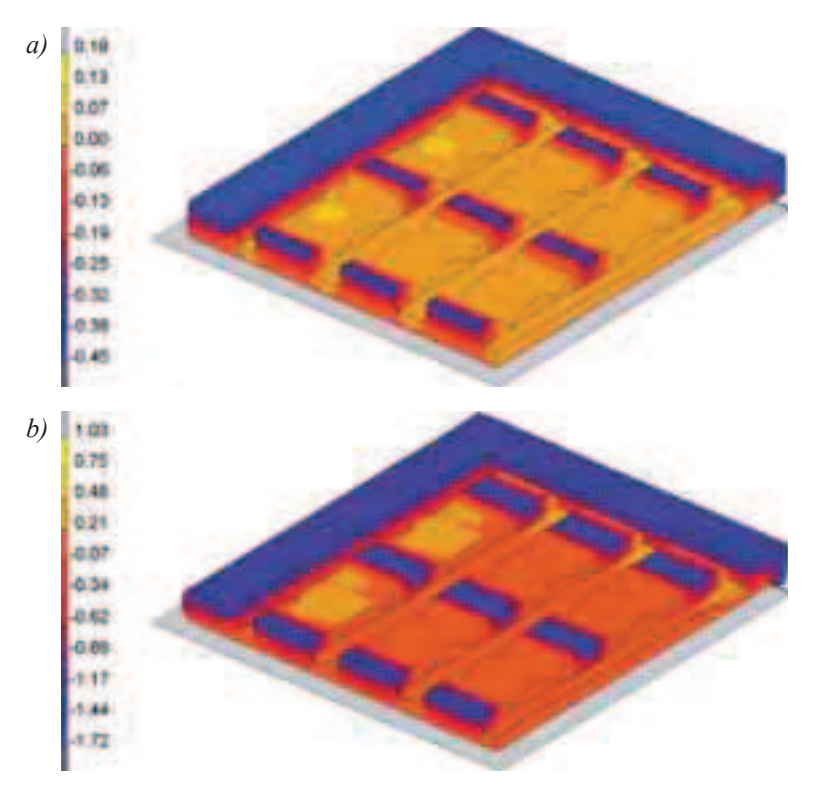


Fig. 11. Contour bands of vertical displacement (mm) for the pad under force P_1 (a) and P_2 (b)

Acknowledgements

Thanks are due to Mrs. Zofia Kowalska, Ph.D. Eng. and Mr. Zbigniew Rodowald, Ph.D. Eng. from the Material and Construction Elements Research Laboratory at the Railway Institute for their guidance and comments.

References

- [1] Sładkowski, A., *Modelling of the Deformation of Elastic Pads for Rail Fastenings*, Transport Problems, Vol. 4, No. 1, pp. 63–70, 2009.
- [2] http://www.railway-technology.com/contractors/rail/plastwil, last retrieved on February 9, 2011.
- [3] Standard Test Methods for Vulcanized Rubber and Thermoplastic Elastomers Tension, ASTM Standard D412 98a (Reapproved 2002), United States 2002.
- [4] Standard Test Methods for Rubber Properties in Compression, ASTM Standard D575 91 (Reapproved 2001), United States 2001.
- [5] Rubber Strain Determination in Compression, Polish Standard No. PN-C-04253:1954, Warsaw 1954.
- [6] Marc 2007 r1, Volume A: Theory and User Information, MSC.Software Corporation, United States 2007.
- [7] Szurgott, P., Boczkowska, A., Kurzydłowski, K. J., Niezgoda, T., *Numerical Strength Analysis of Magnetic Fields Interaction with Elastomer Materials Containing Iron Particles*, Proceeding of the III ECCOMAS Thematic Conference on Smart Structures and Materials, Gdansk, Poland 2007.
- [8] Experimental Elastomer Analysis, User Guide, MSC.Software Corporation, United States 2005.
- [9] Railway applications Track Test Methods for Fastening Systems Part 9: Determination of Stiffness, Polish Standard No. PN-EN 13146-9, Warsaw 2009.
- [10] Marc 2007 r1, Volume B: Element Library, MSC.Software Corporation, United States 2007.